Remote Sensing of Environment 232 (2019) 111319

Contents lists available at ScienceDirect

Remote Sensing of Environment

journal homepage: www.elsevier.com/locate/rse

Accuracy assessment of the TanDEM-X 90 Digital Elevation Model for selected floodplain sites

Laurence Hawker*, Jeffrey Neal, Paul Bates

School of Geographical Sciences, University of Bristol, Bristol, UK

ARTICLE INFO

Edited by Jing M. Chen

Keywords:
Digital Elevation Model
TanDEM-X 90
SRTM
MERIT
Accuracy
Floodplains

ABSTRACT

Freely available Global Digital Elevation Models (GDEMs) are essential for many scientific and humanitarian applications. Recently, TanDEM-X 90 has been released with a global coverage at 3 arc sec resolution. Its release is sure to generate keen interest as it provides an alternative to the widely used Shuttle Radar Topography Mission (SRTM) DEM, especially for flood risk management as for low slope floodplains height errors can become particularly significant. Here, we provide a first accuracy assessment of TanDEM-X 90 for selected floodplain sites and compare it to other popular global DEMs – the Shuttle Radar Topography Mission (SRTM) and the error-reduced version of SRTM called Multi-Error-Removed-Improved-Terrain (MERIT) DEM. We characterize vertical height errors by comparing against high resolution LiDAR DEMs for 32 floodplain locations in 6 continents. Results indicate that the average vertical accuracy of TanDEM-X 90 and MERIT are similar and are both a significant improvement on SRTM. We further our analysis by assessing vertical accuracy by landcover, with our results suggesting that TanDEM-X 90 is the most accurate global DEM in all landcover categories tested except short vegetation and tree-covered areas where MERIT is demonstrably more accurate. Lastly, we present the first characterization of the spatial error structure of any TanDEM-X DEM product, and find the spatial error structure is similar to MERIT, with MERIT generally having lower sill values and larger ranges than TanDEM-X 90 and SRTM. Our findings suggest that TanDEM-X 90 has the potential to become the benchmark global DEM in floodplains with careful removal of errors from vegetation, and at this stage should be used alongside MERIT in any flood risk application.

1. Introduction

Spaceborne Global Digital Elevation Models (GDEMs) are an essential source of topographic information for a wide range of studies including glacial mass balance (Berthier et al., 2006), flood inundation modelling (Sampson et al., 2015), vegetation mapping (Simard et al., 2011) and volcanology (Grosse et al., 2012). Freely available high accuracy airborne DEMs (< 10 m horizontal resolution) are only available for a very small proportion of Earth's land surface (~0.005%) (Hawker et al., 2018a), so spaceborne GDEMs offer the best source of topographic information for most of the Earth. Several freely and commercially available global DEM products exist (Table 1) with the Shuttle Radar Topography Mission (SRTM) the most widely used despite its lack of coverage at high latitudes, presence of voids and non-negligible vertical errors. As a result, error-reduced versions of SRTM have been produced (see Table 1).

Recently, a new free-to-download global DEM has been released - TanDEM-X 90 (https://download.geoservice.dlr.de/TDM90/). With a complete global coverage at 3 arc-seconds resolution (~90 m at the equator), TanDEM-X 90 provides an alternative to the existing global DEMs and is set to spark interest amongst scientists seeking to improve the representation of topography in their studies. To date, error assessment of the TanDEM-X DEM has only been carried out on the non-freely available 0.4 arc-second (~12 m) TanDEM-X DEM (Krieger et al., 2007; Rizzoli et al., 2017), with no such assessment of the freely available TanDEM-X 90. Nor has there been any assessment of the spatial pattern of error (spatial error structure), which has important implications for error propagation (Hunter and Goodchild, 1997) and simulation modelling (Kydriakidis et al., 1999). We chose to focus on low slope floodplains because: 1) Flood inundation modelling applications are particularly sensitive to height errors (Horritt and Bates, 2002) and thus it is imperative to select the most accurate representation of terrain to improve the accuracy of flood predictions and thus most effectively guide flood risk management decisions in these areas of increasing exposure to flooding (Jongman et al., 2012; Wing et al., 2018); 2) to avoid additional error from geometric distortion. Therefore, the

* Corresponding author.
E-mail address: Laurence.hawker@bristol.ac.uk (L. Hawker).

https://doi.org/10.1016/j.rse.2019.111319
Received 15 November 2018; Received in revised form 10 July 2019; Accepted 13 July 2019

Table 1
Summary of global DEM (GDEM) products.

	Dataset	Coverage	Acquisition years	Sensor	Wavelength	Resolution (m)	Vertical accuracy	Reference
Free global DEMs	ALOS AW3D30 v.2.1	82°S - 82°N	2006–2011	Optical	0.52–0.77 μm	30	4.4 m (RMSE)[a]	Tadono et al. (2014); Takaku and Tadono (2017)
	ASTER GDEM v.2	83°S - 83°N	2000–2011	Optical	0.78–0.86	30	17 m (95% conf.)[b]	Tachikawa et al. (2011a)
	GMTED2010	Entire Earth	Completed 2010	Derived from 11 sources of elevation information		250,500,1000	26 m (RMSE)[c]	Danielson and Gesch (2011)
	SRTM	56°S - 60°N	2000	SAR C Band	5.66 cm	30,90	6 m (MAE)[d]	Farr et al. (2007)
	TanDEM-X 90	Entire Earth	2010–2015	SAR X Band	3.1 cm	30,90	Unknown	Rizzoli et al. (2017)
Error reduced versions of SRTM	EarthEnv	60°S - 83°N		ASTER & SRTM		90	4.15 m (RMSE)[e]	Robinson et al. (2014)
	NASADEM			Expected release late 2018				Crippen et al. (2016)
	MERIT	Entire Earth		AW3D30, SRTM & Viewfinder Panorama		90	5 m (LE90)[f]	Yamazaki et al. (2017)
	Bare-Earth SRTM			Same as SRTM		90	5.9 m (RMSE)[g]	O'Loughlin et al. (2016)
	No Name			Same as SRTM		90	1 m reduction in RMSE[h]	Zhao et al. (2018)
	Viewfinder Panorama	Entire Earth		ASTER, SRTM & Other Sources		90	Not Reported	de Ferranti (2014)
Commercial global DEMs	ALOS AW3D	82°S - 82°N	2006–2011	Optical	0.52–0.77um	5	2.7 m (RMSE)[i]	Takaku and Tadono (2017)
	PlanetDEM 30 Plus	Entire Earth		Same as SRTM		30	Not reported	PlanetObserver (2015)
	NEXTMap World 10	Entire Earth		Not Reported		10	10 m (LE95)[j]	InterMap (2018)
	WorldDEM	Entire Earth	2010–2015	SAR X Band	3.1 cm	12	< 1.4 m (RMSE)[k]	Rizzoli et al. (2017)

N.B. Older Global DEMs ACE GDEM (Berry et al., 2000) and GTOPO30 (Gesch et al., 1999) were not included in the table as these products have been superseded by more recent GDEMs.

[a] Tadono et al. (2016) (v1.1).
[b] Tachikawa et al. (2011b).
[c] Danielson and Gesch (2011).
[d] Rodriguez et al. (2006).
[e] Robinson et al. (2014).
[f] Yamazaki et al. (2017).
[g] O'Loughlin et al. (2016).
[h] Zhao et al. (2018).
[i] Takaku et al. (2016).
[j] InterMap (2018).
[k] Wessel et al. (2018).

aim of this article is to provide a comprehensive accuracy assessment of the TanDEM-X 90 DEM in floodplains areas to help users chose the most suitable global DEM for their application. Therefore, we ask the following four questions:

- What is the vertical error of TanDEM-X 90 DEM over low slope floodplains, and how does this compare to other free global DEMs?
- How does the vertical error of TanDEM-X 90 DEM differ between floodplain landcover types?
- Does the vertical error of TanDEM-X 90 DEM vary by floodplain slope and aspect?
- What is the spatial error structure of TanDEM-X 90 DEM in floodplain zones?

To answer these questions, we assess TanDEM-X 90 against high-resolution airborne LiDAR; with the high-resolution LiDAR DEM considered the reference data. Error assessment is made for 32 floodplain locations across 6 continents, with results compared to the widely used SRTM DEM, and an error reduced version of SRTM called MERIT (Multi-Error-Removed-Improved-Terrain), both at 3 arc-second resolution. We justify comparing to MERIT and SRTM at 3 arc sec as both these products are freely available like TanDEM-X 90 and are at the same resolution. In this way we avoid the well-documented influence of horizontal resolution on vertical error (Gao, 1997; Kienzle, 2004; Vaze et al., 2010).

It is crucial for the reader to note that TanDEM-X 90 is a Digital Surface Model (DSM), created from averaging the TanDEM-X 0.4 arc-second DEM. This means that the Earth's surface height is measured including any surface objects, and the data do not represent the bare surface (or Digital Terrain Model (DTM)). In other words, the elevation corresponds to the reflectance surface of the X-band signal. While X-band can penetrate clouds and is unaffected by day/night conditions, the signal is reflected from a surface (e.g. roof of a building, the top of a tree or the bare earth), thus giving an elevation of the surface and not the terrain. However, the X-band signal can partially penetrate vegetation with the scattering centre in trees typically found in the upper part of the vegetation as opposed to at the crown, with the scattering properties also dependent on tree species (Schlund et al., 2014). Like, TanDEM-X 90, SRTM is also a DSM, while MERIT can be considered a DSM with approximated vegetation correction as vegetation artefacts (but not buildings) have been removed from the source SRTM data set (Yamazaki et al., 2017). The high-resolution LiDAR elevation models that are acting as a reference are DTMs. Unlike MERIT, LiDAR DTMs are generated based on ground returns. LiDAR DTMs were used instead of LiDAR DSMs for three reasons: 1) Most applications (e.g. flood modelling) require a bare-earth surface representation of terrain; 2) A DSM is more likely to vary over time (e.g. deforestation, urbanization), while a DTM remains relatively constant over time, so the comparison is more consistent; 3) LiDAR DSMs were not available for all sites. In addition, we are assessing TanDEM-X 90 DEM version 1, which is the initial release (and latest available) but which might contain processing artefacts, outliers, noisy areas and voids (DLR, 2018).

1.1. Background of TanDEM-X

The TanDEM-X mission produced a 0.4 arc-second DEM that covers all 150 million km^2 of the Earth's landmasses from pole to pole (Krieger et al., 2007; Rizzoli et al., 2017; Zink et al., 2014). In its 0.4 arc-second form, TanDEM-X has been used in a number of applications including archaeology (Erasmi et al., 2014), agricultural (Erten et al., 2016), flooding (Archer et al., 2018; Mason et al., 2016), forest mapping (Martone et al., 2018), glaciology (Malz et al., 2018; Rankl and Braun, 2016; Rott et al., 2014), volcanology (Albino et al., 2015; Kubanek et al., 2015; Poland, 2014; Rossi et al., 2016) and urban studies (Rossi and Gernhardt, 2013). Elevations were derived by single pass Synthetic Radar Aperture (SAR) interferometry. Pairs of SAR images were collected at the same time from the twin satellites of TerraSAR-X and TanDEM-X which flew in a close helix formation (300-500 m apart). Images were acquired over a 4-year period between December 2010 and January 2015 (Zink et al., 2014). Bi-static interferometry was used whereby pulses are transmitted by the antenna of one satellite with the backscattered signal received by both satellites. Multiple pairs of images across different seasons were acquired, with all land masses covered at least twice (Borla-Tridon et al., 2013) in order to facilitate the random height accuracies by averaging elevations from each scene (Gonzalez and Brautigam, 2015; Gruber et al., 2016). ICESat spaceborne altimeter data (Zwally et al., 2009) was used to calibrate the DEM (Rizzoli et al., 2017). While SAR imagery has the advantage that it is unaffected by weather or day/night conditions, the measured elevation corresponds to the reflectance surface of the X-band signal. An intermediate DEM product (IDEM) was released in 2014, but was limited in coverage and was based on only the first year of acquisitions. It took until 2016 for the final 0.4 arc-second product (TanDEM-X 12) to be released (Rizzoli et al., 2017).

Mission specifications for TanDEM-X target a 10 m absolute vertical accuracy (90% linear error, LE90) and a 2 m relative vertical accuracy for slopes < 20%, or 4 m for slopes > 40% (Wessel, 2016). The vertical accuracy of the final TanDEM-X DEM at 0.4 arc-seconds has been assessed based on comparisons with ICESat points (Rizzoli et al., 2017), height error maps (HEM) (Gonzalez and Rizzoli, 2018) or KGPS, GPS and LIDAR measurements (Wessel et al., 2018). Using ICESat data, Rizzoli et al. (2017) calculated a global LE90 value of 3.49 m, or just 0.88 m when forested or ice cells were not considered (RMSE not reported). Based on 14 million KGPS points, Wessel et al. (2018) report RMSE values of 1.29 m. Accuracy measurements based on these KGPS utilized measurements were acquired by mounting a GPS antenna on top of a car and driving along roads so the range of landcover types is limited. By also comparing TanDEM-X to 23,951 GPS benchmark points taken across the USA and to 3 high-resolution LiDAR based DEMs, Wessel et al. (2018) report RMSE values of 1.1 m for short vegetation, 1.4 m for developed vegetation and 1.8 m for forests. Most recently, Gonzalez and Rizzoli (2018) used Height Error Maps (HEM) maps to estimate relative height accuracy (or random error), reporting a global value of 1.25 m (thus below the mission specification of 2 m), with the relative height error larger in landcover associated with forests. TanDEM-X has also been compared to other global DEMs (except MERIT), with TanDEM-X performing favorably (Grohmann, 2018). However, to date there has been no vertical accuracy assessment of the TanDEM-X 90 product or comparison of it to other freely available global DEMs at 3 arc-second. Neither has there been any quantification of the spatial error structure for any TanDEM-X product.

Despite the improved accuracy and finer horizontal resolution compared to other global DEMs, the number of applications using TanDEM-X at 0.4 arc-seconds has been limited. This is due to the TanDEM-X at 0.4 arc-seconds only being freely available (currently) upon approval of a scientific proposal, with the quota limited to an area of 100,000km^2. As a result, users have typically stuck with using the SRTM product or increasingly the MERIT DEM or ALOS AW3D30 DEM. However, the ease of access to the new TanDEM-X 90 overcomes the access limitations, so it is important to understand the accuracy of TanDEM-X 90 and how it relates to other global DEMs so users can make an informed decision whether to switch to TanDEM-X 90 in floodplains.

1.2. Study areas

To assess the accuracy of a DEM a reference dataset is needed. According to Maune (2007, pp.407), the accuracy of the reference dataset should be at least three times more accurate than the DEM being assessed. The TanDEM-X mission set a 10 m LE90 absolute error requirement, which results in a required LE90 error of 3.3 m for a reference dataset, leading to a Standard Deviation (STD) accuracy

requirement of < 2 m.

For this study we chose to use high resolution (< 10 m horizontal posting) LiDAR (Light Detection and Ranging) DEMs as a reference dataset. We justify using LiDAR based DEMs for 3 reasons: 1) LiDAR typically has a vertical accuracy of < 20 cm which easily fulfils the accuracy requirement; 2) the spatial distribution of LiDAR elevation values (i.e. on a regular grid) means that calculating the spatial error structure is less susceptible to pixel sparsity; 3) the LiDAR DEMs used provide a new set of validation sites and differ from the ICESat or GPS orientated approaches that have been used in previous TanDEM-X accuracy assessments (Baade and Schmullius, 2016; Wessel et al., 2018). LiDAR DTMs were used for all sites as this study is concerned with assessing error against terrain height, as well as DSMs not being available for all sites.

In total, we use high resolution LiDAR DEMs from 32 locations located across 6 continents. We used the GFPLAIN250m floodplain delineation dataset to guide our choice of site selection (Nardi et al., 2019). All sites needed to be covered by MERIT, SRTM and TanDEM-X 90 DEMs for comparison. Sites range from relatively pristine delta environments (Wax Lake, USA) to urban centres (Piriàpolis, Uruguay) to tropical catchments (Ba, Fiji). The cumulative area of all the high-resolution reference DEMs used is 11,477 km^2 (or 1,416,910 90 m pixels) (Fig. 1).

2. Analysis of DEM error

In DEM accuracy assessments, the vertical height error is calculated by subtracting the reference elevation from the DEM under assessment.

$$\Delta h_i = h_{i,GDEM} - h_{i,ref} \quad (1)$$

where Δh_i is the vertical height error of pixel i, $h_{i,\ GDEM}$ is elevation of a GDEM pixel and $h_{i,\ ref}$ is the elevation of a reference DEM pixel. We assess DEM accuracy using mean error (ME), mean absolute error (MAE), root mean square error (RMSE), median, standard deviation (STD) and skewness. RMSE is a quadratic metric and weights large errors more than small errors. MAE on the other hand is a linear measure, with all values contributing equally to the overall score. We justify using RMSE as it is the standard (although contested) accuracy metric for DEMs and we have a large number of reference points (> 1.4 million) which overcomes the frequent criticism that RMSE values are often computed by a limited sample of reference points (Carlisle, 2005; Fisher and Tate, 2006; Höhle and Höhle, 2009; Wood, 1996). Other accuracy measures typically used in mission specifications (e.g. Wessel (2016)) and other DEM accuracy studies are included in supplementary material.

$$ME = \frac{1}{n}\sum_{i=1}^{n} h_{i,GDEM} - h_{i,ref} = \frac{1}{n}\sum_{i=1}^{n} \Delta h_{i,ref} \quad (2)$$

$$MAE = \frac{1}{n}\sum_{i=1}^{n} |h_{i,GDEM} - h_{i,ref}| = \frac{1}{n}\sum_{i=1}^{n} |\Delta h_{i,ref}| \quad (3)$$

$$RMSE = \sqrt{\frac{1}{n}\sum_{i=1}^{n} \Delta h_{i_{ref}}^2} \quad (4)$$

$$STD = \sqrt{\frac{1}{n-1}\sum_{i=1}^{n} (\Delta h_{i_{ref}} - ME)^2} \quad (5)$$

$$Skewness = \frac{1}{n}\sum_{i=1}^{n} ((h_{i,GDEM} - h_{i,ref}) - ME) \Bigg) \Big/ \left[\frac{1}{n}\sum_{i=1}^{n} ((h_{i,GDEM} - h_{i,ref}) - ME) \right)^2 \Bigg]^{\frac{3}{2}} \quad (6)$$

While the above metrics are a useful summary of vertical error in DEMs, they give a single global measure of deviations and thus do not describe the spatial pattern of error (Fisher and Tate, 2006; Monckton, 1994; Wechsler, 2007).

2.1. Spatial structure of error

Tobler's First Law of Geography states that 'nearby things are more similar than distant things' (Tobler, 1970). While a global average error can be small, local errors can be large and also spatially autocorrelated (Holmes et al., 2000). The spatial structure of error is seldom reported for global DEMs (Fisher and Tate, 2006; Wechsler, 2007), with only several studies for SRTM (Hawker et al., 2018b; LaLonde et al., 2010; Rodriguez et al., 2006; Shortridge, 2006; Shortridge and Messina, 2011) and just one for MERIT (Hawker et al., 2018b).

The spatial structure of DEM error is calculated using semi-

Fig. 1. Location of study sites.

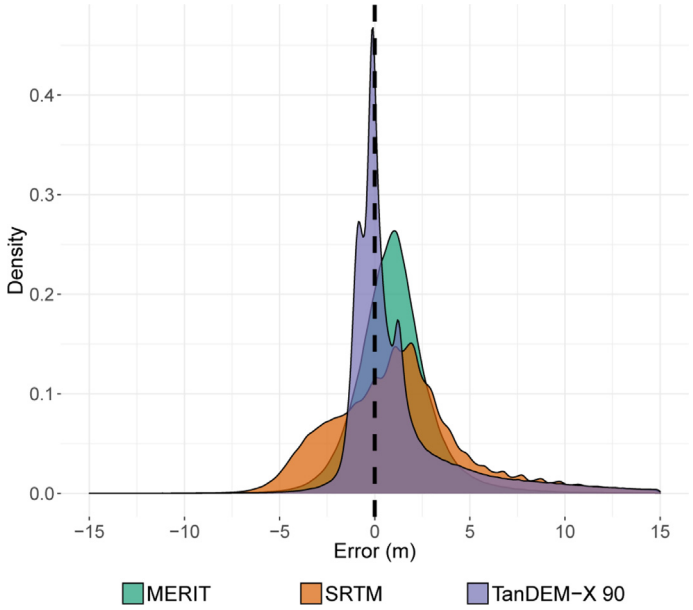

Fig. 2. Distribution of vertical error for MERIT, SRTM and TanDEM-X 90. The x axis has been restricted to −15 to +15 m for visualisation. The y axis is the distribution of the error (GDEM – Reference LiDAR).

Table 2
Descriptive statistics for MERIT, SRTM and TanDEM-X 90 (outliers ± 15 m).

DEM	No. of points	ME (m)	MAE (m)	RMSE (m)	STD (m)	Median (m)	Skewness
MERIT	1,411,475	1.09	1.69	2.32	2.04	0.99	0.80
SRTM	1,389,850	1.30	2.92	3.91	3.69	1.13	0.73
TanDEM-X 90	1,375,407	1.06	1.74	3.10	2.91	0.13	2.09

variograms (Curran, 1988; Deutsch and Journel, 1998; Goovaerts, 1997; Wechsler and Knoll, 2006). We use the method from Hawker et al. (2018b) which is briefly summarised here. A semi-variogram is fitted to the difference map (i.e. SRTM/MERIT/TanDEM-X 90 - LIDAR), with stationarity and isotropy assumed based on testing with directional semi-variograms. The semi-variogram is defined as:

$$\gamma(h) = \frac{1}{2}\left[\{X(s) - X(s')\}^2 \; where \; ||s - s'|| = h \right. \tag{7}$$

where s and s' are vectors of spatial coordinates, X is the difference in elevation at location s between LiDAR and SRTM/MERIT/TanDEM-X 90 and h is the 'lag' or distance between locations measured in decimal degrees. Calculating empirical semi-variograms is interesting in its own right, but by fitting a model semi-variogram to the data an ensemble of plausible DEMs can be simulated (Deutsch and Journel, 1998; Goovaerts, 1997; Hawker et al., 2018b; Holmes et al., 2000). There is no best way to fit semi-variogram models, but the chosen model should capture the main spatial features while not over-fitting (Goovaerts, 1997). Upon inspection of the empirical semi-variograms and a comparison between semi-variogram models, we chose a double-exponential shape model with the form:

$$\gamma(h) = \sigma_1^2\left\{1 - \exp\left(\frac{-h}{a_1}\right)\right\} + \sigma_2^2\left\{1 - \exp\left(\frac{-h}{a_2}\right)\right\} \tag{8}$$

where a_1, a_2 represent the range, ${\sigma_1}^2$ the 'near' component (~500 m) and ${\sigma_2}^2$ the 'far' component (~1000 m). For more information the reader is referred to Hawker et al. (2018b). From the fitted semi-variogram, the sill and the range parameters can be calculated, with the sill referring to the semi-variance value at which the semi-variogram levels off and is the marginal standard deviation, and the range is the distance at which the semi-variogram effectively reaches the sill value, with pairs of points beyond this distance not spatially correlated.

3. Data

3.1. Reference data

High-resolution LIDAR DEMs for 32 locations were acquired to use as the reference data. Further details of the datasets used, including acquisition time can be found in the supplementary materials. All reference DEMs were resampled to the global DEM resolution (90 m) using bilinear resampling.

3.2. Global DEMs

The TanDEM-X 90 product can be freely downloaded from https://download.geoservice.dlr.de/TDM90/ after a simple registration procedure. Each TanDEM-X 90 DEM is available in 1° × 1° tiles. TanDEM-X is unusual amongst global DEMs as each downloaded tile comes with a comprehensive list of 7 auxiliary files – a height error map (HEM), a water indication mask (WAM), a coverage map (COV), a consistency mask (COM), a layover and showdown mask (LSM) and 2 amplitude mosaic layers. Further details of these auxiliary files can be found in Wessel (2016). To compare with the TanDEM-X 90 data, we obtained MERIT DEM (Yamazaki et al., 2017) tiles from http://hydro.iis.u-tokyo.ac.jp/~yamadai/MERIT_DEM/ and CGIAR-CSI (Consortium for Spatial Information) SRTM 4.1 (Jarvis et al., 2008) tiles from http://srtm.csi.cgiar.org/Index.asp. The MERIT DEM was created by using multiple satellite data sets and filtering techniques to identify and reduce absolute bias, stripe noise, speckle noise and tree height bias from SRTM. Therefore, MERIT can be considered an error-reduced version of SRTM, with accuracy assessments suggesting a significant improvement over SRTM (Chen et al., 2018; Hawker et al., 2018b) and could thus be

Table 3
Descriptive statistics for MERIT, SRTM and TanDEM-X 90 for all locations (outliers ± 15 m).

Location	DEM	No. of points	ME (m)	MAE (m)	RMSE (m)	STD (m)	Median (m)	Skewness
Adolpho Ducke	MERIT	1311	11.30	11.30	11.50	2.10	11.48	−0.46
	SRTM	55	14.24	14.24	14.26	0.82	14.52	−2.45
	TanDEM-X 90	141	9.60	9.89	10.74	4.84	11.31	−1.22
Amberley	MERIT	9871	1.86	1.99	2.44	1.59	1.66	0.88
	SRTM	9817	2.16	2.27	3.12	2.25	1.68	1.73
	TanDEM-X 90	9688	1.02	1.13	2.48	2.26	0.16	3.41
Ba	MERIT	6997	0.34	1.22	1.70	1.66	0.42	−0.38
	SRTM	6919	3.54	3.61	4.43	2.67	2.89	0.93
	TanDEM-X 90	6997	2.08	2.12	2.92	2.05	1.35	1.12
Burdekin	MERIT	44,985	2.64	2.70	2.90	1.22	2.66	−0.47
	SRTM	44,418	3.43	3.46	3.85	1.76	3.30	0.37
	TanDEM-X 90	44,982	1.75	1.77	2.42	1.68	1.27	1.61
Cadillac	MERIT	30,847	1.10	1.28	1.55	1.08	1.12	−0.18
	SRTM	30,847	−2.20	2.24	2.51	1.20	−2.19	−0.13
	TanDEM-X 90	30,805	−0.40	0.97	1.44	1.38	−0.45	0.47
Cape Town	MERIT	322,770	1.36	1.92	2.52	2.12	1.35	0.17
	SRTM	321,804	2.29	2.49	3.16	2.17	2.09	0.79
	TanDEM-X 90	322,695	0.34	0.89	1.59	1.56	−0.01	1.90
Cauaxi	MERIT	1273	11.47	11.47	11.65	2.06	11.70	−0.61
	SRTM	1408	1.37	2.26	2.80	2.44	1.47	−0.17
	TanDEM-X 90	28	11.93	11.93	12.36	3.29	12.84	−1.87
Ebro	MERIT	22,532	−1.27	1.34	1.55	0.89	−1.22	−0.32
	SRTM	22,516	−1.31	1.52	1.93	1.41	−1.26	−0.49
	TanDEM-X 90	22,524	−0.81	0.93	1.10	0.74	−0.89	4.20
Eel	MERIT	23,787	−0.90	1.86	2.62	2.46	−1.02	1.15
	SRTM	23,376	−1.13	2.77	3.54	3.35	−1.99	2.22
	TanDEM-X 90	22,986	0.25	1.64	2.86	2.85	−0.89	2.98
Kaiapoi	MERIT	23,906	1.11	1.36	1.88	1.51	0.95	1.42
	SRTM	23,579	1.21	1.76	2.76	2.48	0.67	1.95
	TanDEM-X 90	23,638	1.07	1.18	2.42	2.17	0.29	3.24
Kaikoura	MERIT	7809	1.89	2.15	2.55	1.72	1.87	−0.87
	SRTM	7808	2.68	2.83	3.35	2.01	2.44	0.29
	TanDEM-X 90	7793	0.59	0.78	1.75	1.65	0.02	3.79
Kishima	MERIT	12,059	−1.60	1.76	2.09	1.34	−1.57	−0.16
	SRTM	11,982	−3.12	3.22	3.68	1.96	−3.14	0.06
	TanDEM-X 90	12,059	−0.20	0.36	0.50	0.46	−0.24	−0.56
Kushiro	MERIT	24,491	1.07	1.35	1.84	1.49	1.03	1.74
	SRTM	24,453	−0.32	1.52	1.97	1.94	−0.78	1.74
	TanDEM-X 90	24,440	1.07	1.09	1.67	1.29	0.66	3.63
Matsalu	MERIT	31,703	1.07	1.21	1.36	0.84	1.14	−1.22
	SRTM	31,702	2.31	2.31	2.70	1.40	1.97	1.84
	TanDEM-X 90	31,569	1.11	1.18	2.56	2.30	0.24	2.88
Mekong	MERIT	63,748	1.77	1.81	2.15	1.22	1.52	1.46
	SRTM	63,782	1.33	2.20	2.89	2.57	1.08	0.23
	TanDEM-X 90	63,793	1.72	1.73	2.04	1.09	1.35	2.02
Mississippi	MERIT	22,618	1.36	1.52	1.90	1.33	1.28	0.74
	SRTM	22,118	1.32	1.60	2.05	1.56	1.17	0.55
	TanDEM-X 90	22,621	0.23	0.42	0.61	0.57	0.26	−1.06
Nadi	MERIT	15,948	−0.57	1.40	2.06	1.98	−0.27	−1.42
	SRTM	15,925	1.68	2.00	2.54	1.91	1.55	0.10
	TanDEM-X 90	15,951	0.88	1.23	1.88	1.66	0.50	1.08
Notsuke	MERIT	72,991	0.14	1.67	2.50	2.49	−0.20	1.47
	SRTM	70,822	0.43	1.80	2.74	2.70	−0.10	1.66
	TanDEM-X 90	71,317	3.70	3.83	5.44	3.98	2.01	0.86
Otaki	MERIT	11,299	2.42	2.67	3.02	1.80	2.49	−1.19
	SRTM	11,259	2.98	3.02	3.52	1.87	2.75	1.32
	TanDEM-X 90	11,225	0.62	0.95	1.98	1.88	−0.06	3.75
Parnu	MERIT	53,505	1.51	1.59	1.99	1.29	1.31	1.82
	SRTM	52,198	3.91	3.91	5.31	3.60	2.27	1.29
	TanDEM-X 90	51,060	1.95	2.11	3.92	3.39	0.31	1.93
Piriapolis	MERIT	2244	2.06	2.85	3.67	3.04	1.91	0.17
	SRTM	2208	3.10	3.25	4.28	2.94	2.49	1.13
	TanDEM-X 90	2231	1.82	2.05	2.84	2.17	1.63	0.68
Po Delta	MERIT	40,120	−0.57	1.14	1.48	1.37	−0.67	0.63
	SRTM	40,113	−1.85	2.21	2.59	1.80	−2.00	1.63
	TanDEM-X 90	40,117	−1.15	1.54	1.85	1.44	−1.29	2.62
Roanoke	MERIT	89,247	1.66	2.05	2.64	2.05	1.56	0.77
	SRTM	87,159	6.43	6.51	7.39	3.65	6.64	−0.10
	TanDEM-X 90	77,641	3.70	4.17	5.73	4.37	2.89	0.47
Savannah	MERIT	100,219	2.19	2.47	3.22	2.36	1.76	0.77
	SRTM	90,696	4.42	4.66	6.26	4.44	2.86	0.73
	TanDEM-X 90	90,335	2.64	2.93	5.07	4.32	0.12	1.27

(*continued on next page*)

Table 3 (*continued*)

Location	DEM	No. of points	ME (m)	MAE (m)	RMSE (m)	STD (m)	Median (m)	Skewness
Solothun	MERIT	6960	1.49	1.62	2.18	1.59	1.18	1.29
	SRTM	6721	−1.23	2.66	3.62	3.41	−1.60	0.67
	TanDEM-X 90	6778	0.99	1.35	2.43	2.21	0.23	2.00
Surrey	MERIT	56,861	1.71	2.05	2.88	2.32	1.33	1.31
	SRTM	55,597	2.70	3.04	4.35	3.41	1.85	1.26
	TanDEM-X 90	53,917	2.16	2.83	4.29	3.71	1.22	0.96
Tarm	MERIT	13,938	1.46	1.47	1.57	0.57	1.47	−0.16
	SRTM	13,937	−0.17	0.61	0.83	0.81	−0.23	1.81
	TanDEM-X 90	13,792	0.13	0.50	1.04	1.03	−0.09	3.12
Temuka	MERIT	26,909	1.01	1.13	1.59	1.23	0.78	1.63
	SRTM	26,891	0.82	1.19	1.87	1.68	0.49	2.20
	TanDEM-X 90	26,904	0.25	0.46	1.20	1.18	−0.08	5.07
Tewkesbury	MERIT	18,894	0.95	1.21	1.54	1.21	0.94	0.46
	SRTM	18,890	0.45	1.04	1.60	1.54	0.27	1.89
	TanDEM-X 90	18,798	0.21	1.08	1.95	1.94	−0.12	1.98
Vaudreuil Soulanges	MERIT	229,585	0.29	0.84	1.21	1.17	0.22	0.51
	SRTM	229,542	−2.57	3.12	3.50	2.37	−3.00	1.25
	TanDEM-X 90	226,823	0.23	1.65	2.71	2.70	−0.77	2.53
Waterloo	MERIT	17,532	1.13	1.89	2.58	2.32	0.94	0.62
	SRTM	17,480	1.44	2.51	3.56	3.25	0.95	1.02
	TanDEM-X 90	17,243	0.82	2.18	3.28	3.17	0.28	1.39
Wax Lake	MERIT	4516	1.12	1.24	1.51	1.00	1.24	−0.28
	SRTM	3828	1.87	1.99	2.50	1.66	1.67	1.07
	TanDEM-X 90	4516	0.41	0.78	1.63	1.58	0.02	4.11

deemed the most suitable global DEM for most applications. We chose this version of SRTM as it is void filled and has been used in a large number of studies. The reader should also be aware of the elevation products used in this analysis have different acquisition times (MERIT/SRTM 2000; TanDEM-X 2010–2015; LiDAR variable). To minimize the potential impact of temporality we visually inspected each site in Google Earth for any noticeable landcover changes and determined that significant changes had not taken place. The ASTER GDEM was not assessed in this study, as accuracy measurements have been unfavourable when comparing to SRTM (Athmania and Achour, 2014; Rexer and Hirt, 2014).

3.3. Landcover

We obtain landcover information from the Climate Change Institute (CCI) Land Cover Map (Santoro et al., 2017). The CCI Land Cover Map has annual coverage from 1992 to 2015 and is based on MERIS and SPOT-Vegetation datasets. The resolution is approximately 300 m at the equator and there is a total of 37 land cover classes. As SRTM, (and thus MERIT) were acquired in 2000, we used the CCI Land Cover Map from 2000. On the other hand, TanDEM-X 90 was acquired between 2010 and 2015, so we used the land cover map from 2010. This was necessary as some land cover changed within the decade between the DEM acquisitions.

4. Method

4.1. Datum conversion

TanDEM-X 90 elevations are referenced to the WGS84(G1150) ellipsoid, while MERIT/SRTM elevations are orthometric heights referenced to the EGM96 Geoid. Thus, to compare elevations, TanDEM-X 90 elevations were transformed to the EGM96 Geoid using the vdatum version 3.9 software (NOAA, 2018). Datum levels for the reference DEMs were also transformed as necessary.

4.2. Water masking

Water surfaces in interferometric radar data show a low amount of coherence due to temporal decorrelation and low backscatter, and thus elevation values over water surfaces are often noisy (Wendleder et al., 2013). Therefore, water pixels are masked as non-valid in all DEMs. In the auxiliary files of TanDEM-X 90 a Water Indication Mask (WAM) is included. Values in the WAM file are coded as a bit mask where values correspond to the number of acquisitions with detected water by thresholds of the SAR amplitude or coherence. Islands smaller than 1 ha (1×10^4 m^2) and water bodies smaller than 2 ha (2×10^4 m^2) are excluded in the WAM file. Values from 3 to 32 are when water is detected based on the amplitude only, while 33–127 are when water is detected based on coherence thresholds. When values are from 33 to 64, water is detected on only a single occasion. Further details on the bit mask of the WAM file can be found in Wessel (2016). After an analysis of the WAM files, we chose a byte value of > 65 to use as a water mask with matching pixels in the TanDEM-X 90 DEM masked as non-valid. Our chosen value matched well with satellite imagery and matches the value used by Grohmann (2018).

4.3. Error maps

Elevation error maps were created by subtracting the reference DEM from the global DEM (MERIT/SRTM/TanDEM-X 90). These maps are useful for visualising the spatial distribution of errors and allow for an inference on the causes of the error, especially when compared to satellite imagery. Error maps for TanDEM-X 90 can be found in the supplementary materials.

5. Results and discussion

5.1. Vertical accuracy

The vertical accuracy of TanDEM-X 90 is compared to MERIT and SRTM for 32 sites. The distribution of vertical error by DEM is plotted in Fig. 2 and the descriptive statistics can be found in Table 2. We remove outliers which we classify as pixels with errors ± 15 m which is approximately 3 standard deviations (i.e. the 3 sigma rule).

Fig. 2 reveals that the vertical errors in MERIT and SRTM have a more normal shape, being unimodal and symmetric, whereas TanDEM-X 90 errors have a strikingly bimodal distribution The 'jagged' nature of the SRTM distribution is likely to be due to elevation values being given as integers.

Table 2 reveals that TanDEM-X 90 and MERIT have a similar accuracy. Both MERIT and TanDEM-X 90 are more accurate than SRTM.

Table 4
Descriptive statistics for vertical error in SRTM, MERIT and TanDEM-X 90 by landcover category (with outliers removed). The DEM with the best vertical accuracy is highlighted in grey.

Category	DEM	No. of Points	ME (m)	MAE (m)	RMSE (m)	STD (m)	Median (m)	Skewness
Bare	MERIT	7529	0.36	1.65	2.22	2.19	0.30	0.00
	SRTM	6860	0.33	2.26	2.99	2.97	0.24	0.54
	TanDEM-X 90	6619	0.03	1.17	2.04	2.04	-0.32	2.33
Short Vegetation	MERIT	771838	0.71	1.35	1.83	1.68	0.70	0.28
	SRTM	769432	-0.02	2.42	3.07	3.07	-0.04	0.54
	TanDEM-X 90	762798	0.36	1.22	2.12	2.09	-0.13	2.59
Shrubland	MERIT	155665	1.24	1.77	2.34	1.98	1.23	0.44
	SRTM	154140	2.12	2.51	3.34	2.58	1.90	1.14
	TanDEM-X 90	147935	0.48	0.95	1.95	1.89	0.07	3.13
Sparse Vegetation	MERIT	1948	1.79	2.25	3.09	2.52	1.59	0.94
	SRTM	1907	2.15	2.61	3.54	2.82	1.85	0.94
	TanDEM-X 90	1702	-0.01	0.68	1.30	1.30	-0.18	3.96
Tree Cover	MERIT	304786	1.61	2.26	3.12	2.67	1.35	0.93
	SRTM	291352	4.17	4.78	6.04	4.37	3.55	0.30
	TanDEM-X 90	251150	3.69	4.07	5.68	4.32	2.53	0.67
Urban	MERIT	108387	2.29	2.39	2.79	1.60	2.24	0.57
	SRTM	107958	2.11	2.48	3.14	2.32	2.01	0.67
	TanDEM-X 90	149233	1.19	1.50	2.38	2.06	0.76	1.80

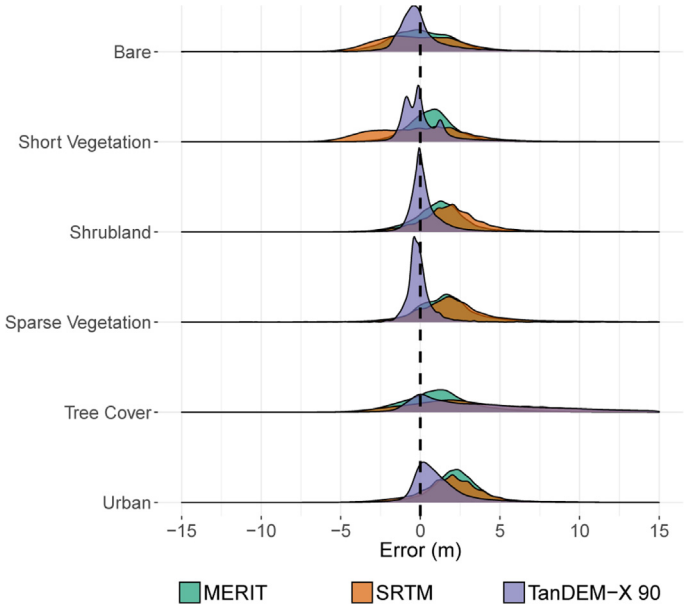

Fig. 3. Density plot of error by landcover category. The y axis is the probability density function of the vertical error (GDEM – Reference LiDAR).

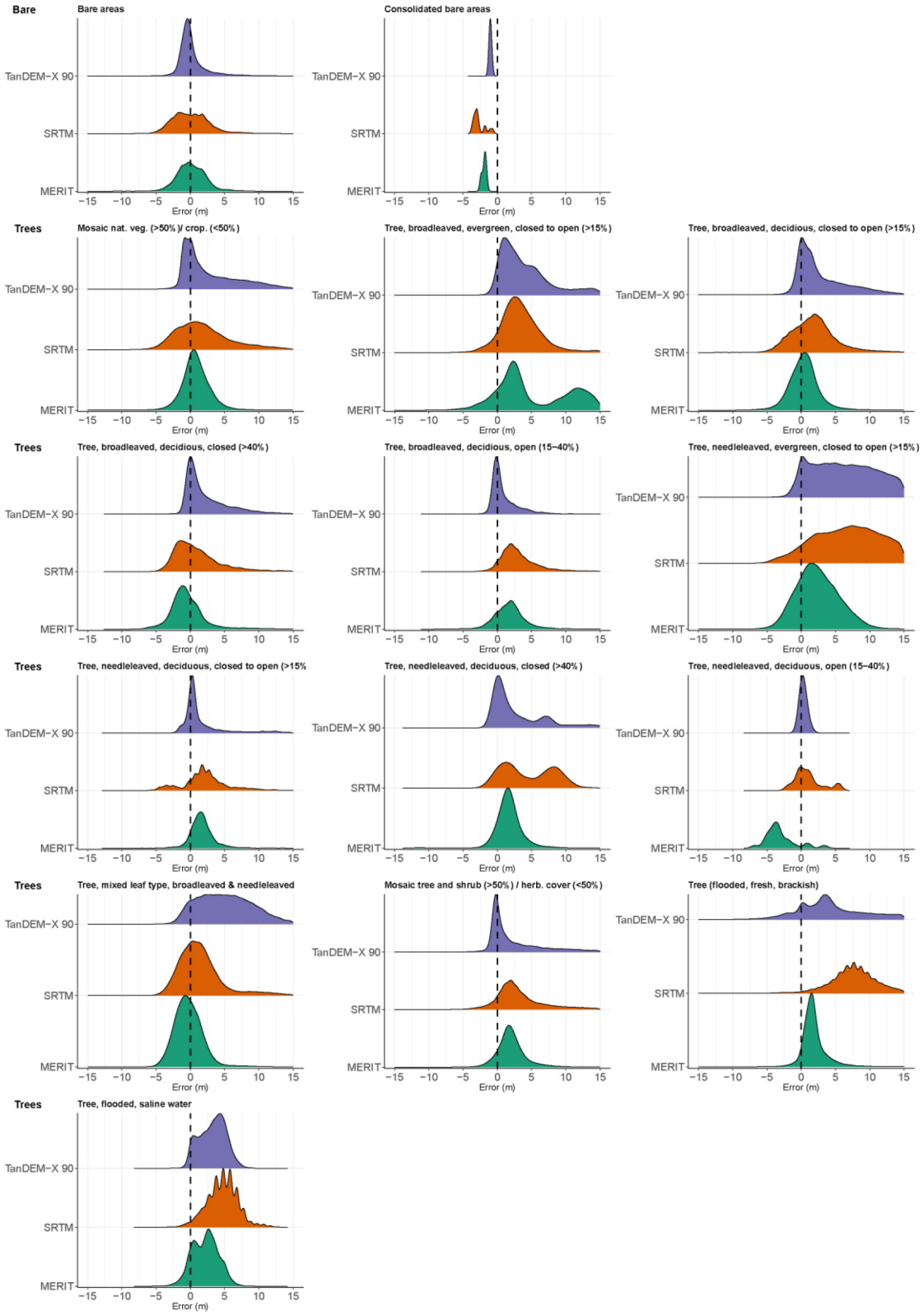

Fig. 4. Distribution of vertical error for MERIT, SRTM and TanDEM-X 90 by CCI landcover class. Landcover classes in the bare areas and tree cover categories are shown. The x axis have been restricted to −15 to +15 m for visualisation.

TanDEM-X 90 has a mean error (ME) of 1.06 m, mean absolute error of 1.74 m and RMSE of 3.16 m. While these metrics are greater than those reported by Wessel et al. (2018) when they compared to KGPS and GPS points, our values align more closely with their values when comparing to high-resolution DEMs. It should be noted that Wessel et al. (2018) used TanDEM-X at 12 m for their analysis. MERIT has a marginally higher ME (1.09 m), but lower MAE (1.69 m) and RMSE (2.32 m) than TanDEM-X 90. MERIT is slightly positively skewed (0.80), while TanDEM-X has a relatively large positive skew (2.09). The density distribution of errors in Fig. 2 shows a narrower spread of errors for

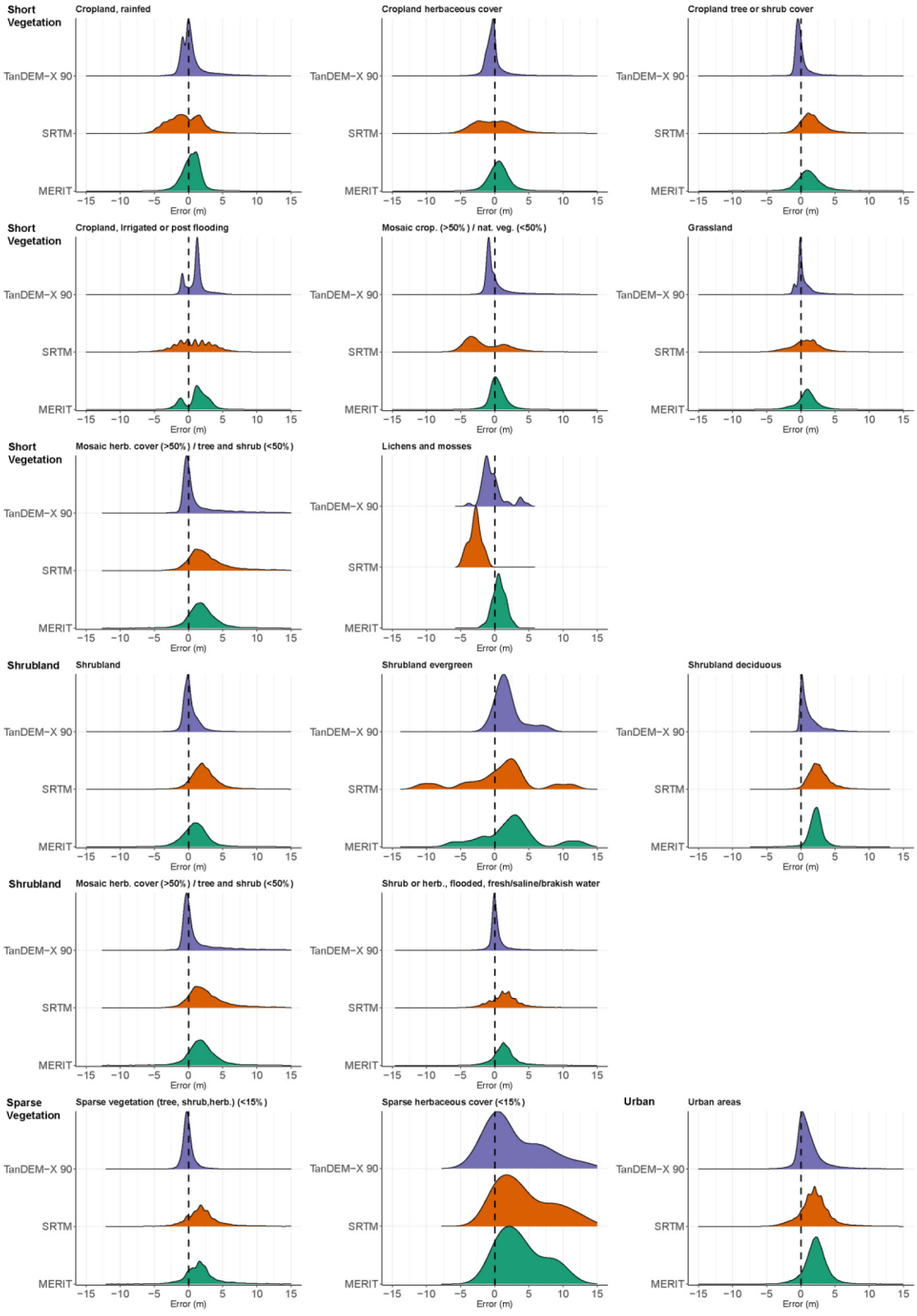

Fig. 5. Distribution of vertical error for MERIT, SRTM and TanDEM-X 90 by CCI landcover class. Landcover classes in the short vegetation, sparse vegetation, shrubland and urban categories are shown. The x-axis has been restricted to −15 m to +15 m for visualisation.

TanDEM-X 90 compared to MERIT. This is also evidenced by the lower median values (0.13 m for TanDEM-X 90 compared to 0.99 m for MERIT). If considering the density distribution of errors, median values and mean error values, TanDEM-X 90 is the most accurate GDEM. However, if the popular RMSE metric is only considered, MERIT is the most accurate GDEM. RMSE is a quadratic metric that puts greater weight on large error values, thus although most of the errors in TanDEM-X 90 are small, the larger errors are distorting the RMSE score, despite the use of removing outliers using the 3-sigma rule. For all metrics, SRTM is less accurate (ME of 2.16 and RMSE of 4.03) than

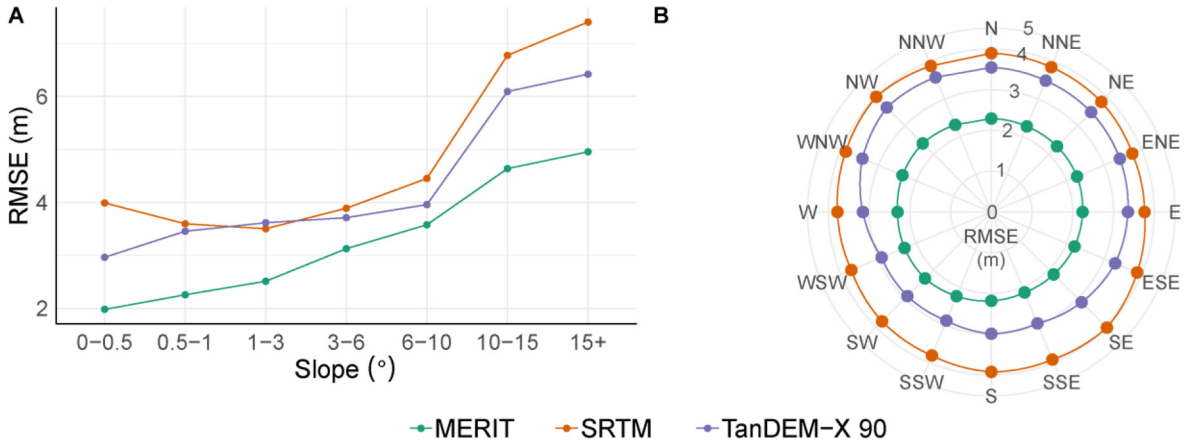

Fig. 6. Vertical error for all locations measured by root mean square error (m) for A) Slope and B) Aspect.

Table 5
Vertical error in RMSE by slope in degrees for all locations.

Slope (°)	0–0.5	0.5–1	1–3	3–6	6–10	10–15	15+
Description	Flat	Nearly flat	Very gentle slope	Gentle slope	Moderate slope	Steep slope	Very steep slope
MERIT	1.98	2.30	2.56	3.15	3.59	4.64	4.95
SRTM	4.01	3.72	3.61	3.93	4.47	6.79	7.40
TanDEM-X 90	2.92	3.18	3.34	3.58	3.90	6.07	6.42
No. of points	766,225	178,444	236,298	81,449	21,367	3218	1141

Table 6
Vertical error in RMSE by aspect for all locations. Aspect directions calculated on a 16 point compass.

Direction	Count	MERIT	SRTM	TanDEM-X 90
N	69,418	2.30	3.98	3.33
NNE	69,187	2.30	3.94	3.28
NE	71,658	2.31	3.93	3.28
ENE	72,963	2.31	3.86	3.22
E	81,790	2.28	3.88	3.16
ESE	91,113	2.24	3.96	3.14
SE	96,433	2.18	4.07	3.04
SSE	95,650	2.14	3.95	2.87
S	89,350	2.18	3.94	2.92
SSW	83,595	2.23	3.82	2.83
SW	82,980	2.30	3.80	2.87
WSW	84,213	2.30	3.74	2.84
W	81,866	2.30	3.81	3.04
WNW	75,379	2.36	3.92	3.27
NW	72,782	2.39	4.06	3.45
NNW	69,768	2.32	3.94	3.38

MERIT and TanDEM-X 90 suggesting that the error removal procedure in MERIT has been effective.

We also present the descriptive statistics for all 32 locations (Table 3). All DEMs have a poor vertical accuracy for the Roanoke and Savannah sites as well as Adolpho Ducke and Cauaxi in the Amazon rainforest, with the greatest errors for the former sites having a CCI landcover of 'Tree, needle-leaved, evergreen, closed to open (> 15%)' The vertical accuracy of TanDEM-X 90 is largely comparable to MERIT, with the TanDEM-X 90 performing particularly well in the Mississippi, Tarm and Temuka sites. In tree-covered locations such as Ba in Fiji, the MERIT DEM has a better vertical accuracy than SRTM and TanDEM-X 90 suggesting the vegetation removal procedure has been effective. In addition, we can also compare the differences between TanDEM-X 12 and TanDEM-X 90 as both this study and the study of Wessel et al. (2018) used Cape Town. This study only considered pixels with a slope of 10° or less and found a ME of 0.34 m and RMSE of 1.59 m. This compares to a ME of 0.30 m and RMSE of 3.89 m in Wessel et al. (2018).

5.2. Vertical accuracy by landcover

Using the CCI landcover classes, we assess the vertical error per landcover class. In Table 4 we provide a summary of descriptive statistics for landcover classes split into 6 categories - Bare areas, short vegetation, shrubland, sparse vegetation, tree covered areas and urban areas. The DEM with the best vertical accuracy (based on RMSE) is highlighted in green. An additional table of descriptive statistics per individual landcover class (30 out of the possible 37 landcover classes assessed) can be found in supplementary materials. Figs. 3, 4 and 5 show the distribution of vertical error by landcover class.

Contrary to our conclusion in 5.1, TanDEM-X 90 has the best vertical accuracy in 4 out of the 6 landcover categories. TanDEM-X has noticeably smaller errors than MERIT and SRTM in shrubland and sparse vegetation, with RMSE values of 1.95 m and 1.30 m respectively. This compares to RMSE values of 2.34 m and 3.09 m in the next most accurate DEM, MERIT. The distribution of vertical error in short vegetation for TanDEM-X 90 (Fig. 3) has a similar bimodal distribution as when we consider all landcover types (Fig. 2), thus leading us to conclude that either X-band SAR is unable to fully penetrate some short vegetation landcovers or that this is a result of seasonality as TanDEM-X 90 has been produced from images collected across seasons. However, for tree-covered areas, MERIT has a considerably better vertical accuracy with a ME of 1.69 m and RMSE of 3.12 compared to an ME of 3.69 m and RMSE of 5.68 m for TanDEM-X 90. This is unsurprising as MERIT has had the tree height bias removed. Our RMSE values for tree-covered areas are higher than those found by Wessel et al. (2018) who report an RMSE value of 1.8 m for forested areas. Indeed, the vertical accuracy of TanDEM-X 90 in tree-covered areas is more like that of SRTM.

We go into further detail in our investigation of the effect of landcover on vertical error by assessing the vertical error by each individual CCI landcover class (Fig. 4, Fig. 5 and supplementary materials). We find that the vertical error distribution and descriptive statistics can vary considerably within each landcover category. For instance, some landcover classes within the tree-cover category can perform reasonably well (e.g. 'Broadleaved, deciduous, open to closed (15–40%)'),

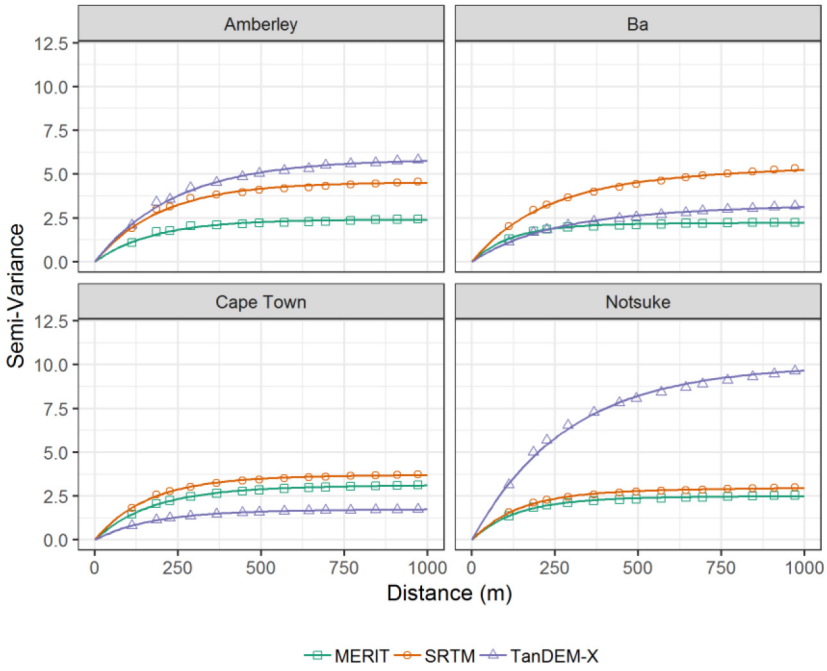

Fig. 7. Selected semi-variograms for the difference between MERIT-LIDAR, SRTM-LIDAR and Tandem-X 90-LIDAR. The 'sill' is the marginal standard deviation in metres and the range is the distance in metres at which the correlation between two points drop to 0.05.

while others have a large positive bias ('needle-leaved, evergreen, closed to open (> 15%)'). This finding concurs with that of Gonzalez and Rizzoli (2018) who find a similar amount of variation with land-cover categories when assessing relative height error.

5.3. Vertical error by aspect & slope

Despite focusing on flat terrain, we further assess vertical accuracy by aspect and slope as sloped areas are found on the edges of floodplains and are important in delineating floodplain boundaries. Aspect and slope are derived from the resampled LiDAR DEM at 3 arc sec, and have been binned into 7 slope categories and 16 compass point directions (Fig. 6, Tables 5 & 6).

The error of TanDEM-X 90 is marginally higher than MERIT but lower than SRTM for all slope categories. For all GDEMs the lowest RMSE values are for the flattest slopes. For TanDEM-X and SRTM, RMSE values increase considerably for 'steep' and 'very steep slopes', while this change is less for MERIT. This is likely due to the error removal process in MERIT which creates a smoother surface. Wessel et al. (2018) also found a considerable rise in RMSE values above slopes of 10° ('steep slope'), although our analysis differs slightly as Wessel et al. (2018) bin all slopes below 10° into 1 category while we separate into 5 bins below 10° owing to our focus on flatter terrain.

Error by aspect for TanDEM-X 90 varies by 0.62 m, with the lowest value in the SSW direction (2.69 m) and the highest in the NW direction (3.45 m). SRTM has a lower variation in RMSE (0.33 m) but higher RMSE values, while MERIT has a smaller variation (0.25 m) and lower RMSE values than TanDEM-X 90. For all DEMs we find the largest error in the NW direction, while the lowest errors were in the southerly and westerly regions. Previous studies also find the largest error in SRTM to be in the NW direction (Gorokhovich and Voustianiouk, 2006; Shortridge and Messina, 2011), while we are unaware of any aspect related error estimations for MERIT or TanDEM-X 90.Similar to Shortridge and Messina (2011), we attribute SRTM and MERIT aspect related error to orientation of the sensor but are currently unable to explain the reason for TanDEM-X 90. Therefore, accuracy is strongly associated with aspect.

5.4. Spatial error

The spatial error structure describes the dependence of error spatially and is of interest for error propagation and DEM simulation. We plot semi-variograms for all locations (Fig. 7) and present semi-variogram parameters by location and landcover class in Table 7 and supplementary materials. To interpret the semi-variogram, low sill values mean the DEM is more accurate, and a large range means the error is more spatially dependent.

Broadly speaking the semi-variograms of TanDEM-X 90 resemble those of MERIT (parameter values in supplementary materials). When assessing by location, MERIT has the lowest sill value for 22 locations, while for TanDEM-X 90 this is 9 (SRTM lowest for Adolpho Ducke). TanDEM-X 90 has the highest range (errors more spatially dependent) for 15 locations as opposed to 12 for MERIT (5 for SRTM). For some locations (e.g. Amberley and Otaki), the semi-variograms of TanDEM-X 90 are more like those of SRTM. There are several exceptions (Notsuke & Roanoke) where the sill values of TanDEM-X 90 are larger than MERIT and SRTM and the range shorter.

We also compare semi-variogram parameters by landcover class. These semi-variograms by landcover class are calculated by selecting elevation pixels that correspond to a landcover class and masking out all the other pixels. To produce semi-variograms, we selected landcover classes per location with a minimum of 600 pixels. The parameters values are in the supplementary materials but we found no discernable pattern.

MERIT generally has lower sill values (0.5–3.4 m, average 1.50 m) and shorter-range values (298–5098 m, average 1382 m) than TanDEM-X 90 (sill 0.4–19.2 m, average 2.74 m; range 298–18,586 m, average 2136 m) and SRTM (sill 0.8–7.2 m, average 2.28 m; range 298–7151 m, average 1334 m). Therefore, MERIT can be said to be more accurate, with errors more spatially independent compared to TanDEM-X 90 and SRTM. TanDEM-X 90 generally has lower sill values for all landcovers except tree covered areas where sill values are higher than MERIT. However, the spatial error structure of TanDEM-X 90 is more like MERIT than SRTM. This is a little surprising because MERIT has been heavily processed and the TanDEM-X 90 version analysed here is a non-void filled product that has had relatively little manipulation.

Table 7
Semi-variogram parameters for MERIT, SRTM and TanDEM-X by location.

Location	DEM	Sill (m)	Range (m)
Adolpho Ducke	MERIT	2.3	298
	SRTM	1.6	389
	TanDEM-X 90	19.2	18,586
Amberley	MERIT	1.6	528
	SRTM	2.1	592
	TanDEM-X 90	2.4	722
Ba	MERIT	1.5	572
	SRTM	2.6	3754
	TanDEM-X 90	2.0	4318
Burdekin	MERIT	1.2	4188
	SRTM	1.5	2382
	TanDEM-X 90	1.4	4121
Cadillac	MERIT	1.1	298
	SRTM	1.2	298
	TanDEM-X 90	1.4	1261
Cape Town	MERIT	1.8	1331
	SRTM	2.0	817
	TanDEM-X 90	1.4	1548
Cauaxi	MERIT	2.4	420
	SRTM	2.4	327
	TanDEM-X 90	3.3	413
Ebro	MERIT	0.7	298
	SRTM	1.1	298
	TanDEM-X 90	0.7	298
Eel	MERIT	1.6	1019
	SRTM	2.8	3421
	TanDEM-X 90	3.0	5675
Kaiapoi	MERIT	1.4	745
	SRTM	2.4	664
	TanDEM-X 90	2.4	686
Kaikoura	MERIT	1.5	470
	SRTM	1.8	872
	TanDEM-X 90	1.6	535
Kishima	MERIT	1.0	1714
	SRTM	1.7	365
	TanDEM-X 90	0.4	450
Kushiro	MERIT	1.2	2274
	SRTM	1.4	1330
	TanDEM-X 90	1.0	1435
Matsalu	MERIT	0.8	3774
	SRTM	1.3	1130
	TanDEM-X 90	2.1	1052
Mekong	MERIT	1.0	1440
	SRTM	2.4	298
	TanDEM-X 90	1.0	499
Mississippi	MERIT	1.3	1438
	SRTM	1.5	470
	TanDEM-X 90	0.6	405
Nadi	MERIT	1.7	298
	SRTM	1.6	313
	TanDEM-X 90	1.4	1837
Notsuke	MERIT	1.6	977
	SRTM	1.8	1419
	TanDEM-X 90	3.2	861
Otaki	MERIT	1.7	1211
	SRTM	1.9	448
	TanDEM-X 90	2.0	574
Parnu	MERIT	1.2	1052
	SRTM	7.2	7151
	TanDEM-X 90	4.0	826
Piriapolis	MERIT	3.4	5098
	SRTM	3.0	874
	TanDEM-X 90	2.3	678
Po Delta	MERIT	1.1	3484
	SRTM	1.7	3076
	TanDEM-X 90	1.4	4786
Roanoke	MERIT	2.0	779
	SRTM	3.6	794
	TanDEM-X 90	5.0	1890
Savannah	MERIT	2.2	4682
	SRTM	5.1	6332
	TanDEM-X 90	5.2	5671
Solothun	MERIT	1.4	647
	SRTM	3.0	613
	TanDEM-X 90	2.0	890
Surrey	MERIT	2.3	1847
	SRTM	3.6	1011
	TanDEM-X 90	4.1	1203
Tarm	MERIT	0.5	551
	SRTM	0.8	657
	TanDEM-X 90	1.1	2208
Temuka	MERIT	1.1	710
	SRTM	1.6	471
	TanDEM-X 90	1.1	863
Tewkesbury	MERIT	1.1	436
	SRTM	1.4	478
	TanDEM-X 90	2.0	707
Vaudreuil Soulanges	MERIT	1.0	624
	SRTM	2.1	541
	TanDEM-X 90	2.8	770
Waterloo	MERIT	2.3	661
	SRTM	3.5	957
	TanDEM-X 90	3.6	802
Wax Lake	MERIT	1.0	1077
	SRTM	1.8	795
	TanDEM-X 90	1.7	3215

6. Conclusions

In this study, we assessed the vertical error and spatial error structure of the recently released TanDEM-X 90 global DEM for 32 floodplain locations across 6 continents. We compared our results to popular existing global DEMs - MERIT and SRTM. Our motivation behind this was to help guide DEM users in choosing the most accurate Global DEM for their application in floodplain areas.

Our findings reveal that TanDEM-X 90 has a MAE of 1.74 m and RMSE of 3.10 m for our 32 floodplain sites. This compares to a MAE of 1.69 m and RMSE of 2.32 m for MERIT and MAE of 2.92 m and RMSE of 3.91 m for SRTM. However, the density distribution of errors and the median values reveals that the accuracy statistics for TanDEM-X 90 are distorted by large errors, with most of the errors close to 0 m. Further investigation into vertical error by landcover class revealed that the vertical error of TanDEM-X 90 is lower for all landcover categories except short vegetation and tree covered areas where MERIT has a considerably lower vertical error. This is likely due to the effective vegetation removal procedure in MERIT and the fact that the X-band SAR of TanDEM-X and SRTM struggles to penetrate tree canopies. However, the vertical error of each landcover class within each landcover category can vary considerably.

We also assessed the vertical error by slope and aspect and found that the vertical error of all GDEMs are lowest in the flattest areas, with the error increasing by slope and increasing most for the steepest slopes (above 10°). The lowest error for TanDEM-X was found in the SSW direction, with all DEMs having the largest errors in the NW direction. Moreover, we present semi-variograms to visualise the spatial error structure of TanDEM-X 90 and find the spatial error structure is visually similar to MERIT, with sill values of TanDEM-X 90 between 0.4 and 19.2 m and range values between 298 and 18,586 m (compared to 0.5–3.4 m and 298-5098 m respectively for MERIT). To our knowledge this is the first time that semi-variograms have been presented for any TanDEM-X 90 DEM product.

Our analysis suggests that when choosing a Global DEM one should consider the predominant landcover in the site. If the site is predominantly tree-covered, the MERIT DEM is likely to be most accurate. For areas of bare ground, shrubland, urban areas and sparse vegetation TanDEM-X 90 has the best vertical accuracy, while for short vegetation, MERIT has a moderately better accuracy. However, the improved vertical accuracy of MERIT in tree-covered areas offsets its moderately

worse vertical accuracy compared to TanDEM-X 90 in other landcover categories. Both MERIT and TanDEM-X 90 have consistently better vertical accuracy than SRTM and thus should be used over SRTM. We also find that the accuracy statistics computed for TanDEM-X 90 are distorted by the presence of a low number of large errors, with the density distribution and median values revealing that most vertical errors are close to 0. Therefore, if these large artefacts are removed, TanDEM-X 90 is likely to be the most accurate GDEM in floodplain locations. It should be noted that the TanDEM-X 90 product assessed here is non-void filled and contains no vegetation or noise removal. Thus, when noise and vegetation artefacts are removed from TanDEM-X 90 there is a distinct possibility that it could become the benchmark in free global DEMs in floodplains.

Funding

This work is funded as part of the Water Informatics Science and Engineering Centre for Doctoral Training (WISE CDT) under a grant from the Engineering and Physical Sciences Research Council (EPSRC), grant EP/L016214/1, and a NERC SHEAR catalyst grant (NE/S006079/1). Paul Bates is supported by a Leverhulme Research Fellowship and Royal Society Wolfson Research Merit award.

Author contributions

LH wrote the manuscript and carried out the data analysis. JN and PB reviewed and provided comments on various drafts as well as advised on the analysis work.

Data

This study uses data from 3 global DEM products – MERIT, SRTM Version 4.1 and TanDEM-X 90 – which are available from https://cgiarcsi.community/data/srtm-90m-digital-elevation-database-v4-1/, http://hydro.iis.u-tokyo.ac.jp/~yamadai/MERIT_DEM/ and https://geoservice.dlr.de/web/dataguide/tdm90/ respectively. These datasets are freely available, but a request must be sent for access for the MERIT Dataset to the author. Details of the LIDAR datasets are found in supplementary materials.

Acknowledgements

We would like to thank Chris Crook (LINZ), Maiza Nara (EMBRAPA-CNPTIA) and Charles Papasodoro (NRCAN/RNCAN) for their help in LiDAR datum conversion. We would also like to thank Jonathan Rougier for his advice on statistics. In addition the work was funded by another NERC Grant (NERC Understanding of the Impacts of Hydrometeorological Hazards in South East Asia Grant (NE/S003061/1)).

Appendix A. Supplementary data

Supplementary data associated with this article can be found in the online version, at doi:https://doi.org/10.1016/j.rse.2019.111319. These data include the Google map of the most important areas described in this article.

References

Albino, F., Smets, B., d'Oreye, N., Kervyn, F., 2015. High-resolution TanDEM-X DEM: an accurate method to estimate lava flow volumes at Nyamulagira Volcano (D. R. Congo). Journal of Geophysical Research: Solid Earth 120, 4189–4207.

Archer, L., Neal, J., Bates, P., House, J., 2018. Comparing TanDEM-X data with frequently used DEMs for flood inundation modelling. Water Resour. Res. 54, 10,205–210,222.

Athmania, D., Achour, H., 2014. External validation of the ASTER GDEM2, GMTED2010 and CGIAR-CSI-SRTM v4.1 free access Digital Elevation Models (DEMs) in Tunisia and Algeria. Remote Sens. 6, 4600–4620.

Baade, J., Schmullius, C., 2016. TanDEM-X IDEM precision and accuracy assessment based on a large assembly of differential GNSS measurements in Kruger National Park, South Africa. ISPRS J. Photogramm. Remote Sens. 119, 496–508.

Berry, P.A.M., Pinnock, R.A., Hilton, R.D., Johnson, C.P.D., 2000. ACE: a new global digital elevation model incorporating satellite altimeter derived heights. In: ERS-Envisat Symposium. 2000.

Berthier, E., Arnaud, Y., Vincent, C., Rémy, F., 2006. Biases of SRTM in high-mountain areas: implications for the monitoring of glacier volume changes. Geophys. Res. Lett. 33.

Borla-Tridon, D., Bachmann, M., Schulze, D., Míguez, C.O., Polimeni, M.D., Martone, M., Böer, J., Zink, M., 2013. TanDEM-X: DEM acquisition in the third year era. International Journal of Space Science and Engineering 1.

Carlisle, B.H., 2005. Modelling the spatial distribution of DEM error. Trans. GIS 9, 521–540.

Chen, H., Liang, Q., Liu, Y., Xie, S., 2018. Hydraulic correction method (HCM) to enhance the efficiency of SRTM DEM in flood modeling. J. Hydrol. 559, 56–70.

Crippen, R., Buckley, S., Agram, P., Belz, E., Gurrola, E., Hensley, S., Kobrick, M., Lavalle, M., Martin, J., Neumann, M., Nguyen, Q., Rosen, P., Shimada, J., Simard, M., Tung, W., 2016. Nasadem global elevation model: methods and progress. ISPRS - International Archives of the Photogrammetry, Remote Sensing and Spatial Information Sciences XLI-B4, 125–128.

Curran, P.J., 1988. The semivariogram in remote sensing an introduction. Remote Sens. Environ. 24, 493–507.

Danielson, J.J., Gesch, D.B., 2011. Global Multi-resolution Terrain Elevation Data 2010 (GMTED2010). In. pp. 1073.

Deutsch, C.V., Journel, A.G., 1998. GSLIB: Geostatistical Software Library and User's Guide, Second ed. Oxford University Press, New York.

DLR, 2018. The TanDEM-X 90m Digital Elevation Model. https://geoservice.dlr.de/web/dataguide/tdm90/.

Erasmi, S., Rosenbauer, R., Buchbach, R., Busche, T., Rutishauser, S., 2014. Evaluating the quality and accuracy of TanDEM-X digital elevation models at archaeological sites in the Cilician Plain, Turkey. Remote Sens. 6, 9475–9493.

Erten, E., Lopez-Sanchez, J.M., Yuzugullu, O., Hajnsek, I., 2016. Retrieval of agricultural crop height from space: a comparison of SAR techniques. Remote Sens. Environ. 187, 130–144.

Farr, T.G., Rosen, P.A., Caro, E., Crippen, R., Duren, R., Hensley, S., Kobrick, M., Paller, M., Rodriguez, E., Roth, L., Seal, D., Shaffer, S., Shimada, J., Umland, J., Werner, M., Oskin, M., Burbank, D., Alsdorf, D., 2007. The shuttle radar topography mission. Rev. Geophys. 45.

de Ferranti, J., 2014. Viewfinder Panorama. http://www.viewfinderpanoramas.org/dem3.html.

Fisher, P.F., Tate, N., 2006. Causes and consequences of error in digital elevation models. Prog. Phys. Geogr. 30, 467–489.

Gao, J.A.Y., 1997. Resolution and accuracy of terrain representation by grid DEMs at a micro-scale. Int. J. Geogr. Inf. Sci. 11, 199–212.

Gesch, D.B., Verdin, K., Greenlee, S.K., 1999. New land surface digital elevation model covers the Earth. EOS Transactions American Geophysical Union 80, 69–70.

Gonzalez, C., Brautigam, B., 2015. Relative height accuracy estimation method for InSAR-based DEMs. IEEE Journal of Selected Topics in Applied Earth Observations and Remote Sensing 8, 5352–5360.

Gonzalez, C., Rizzoli, P., 2018. Landcover-dependent assessment of the relative height accuracy in TanDEM-X DEM products. IEEE Geosci. Remote Sens. Lett. 1–5.

Goovaerts, P., 1997. Geostatistics for Natural Resource Evaluation. Oxford University Press, Oxford.

Gorokhovich, Y., Voustianiouk, A., 2006. Accuracy assessment of the processed SRTM-based elevation data by CGIAR using field data from USA and Thailand and its relation to the terrain characteristics. Remote Sens. Environ. 104, 409–415.

Grohmann, C.H., 2018. Evaluation of TanDEM-X DEMs on selected Brazilian sites: comparison with SRTM, ASTER GDEM and ALOS AW3D30. Remote Sens. Environ. 212, 121–133.

Grosse, P., van Wyk de Vries, B., Euillades, P.A., Kervyn, M., Petrinovic, I.A., 2012. Systematic morphometric characterization of volcanic edifices using digital elevation models. Geomorphology 136, 114–131.

Gruber, A., Wessel, B., Martone, M., Roth, A., 2016. The TanDEM-X DEM mosaicking: fusion of multiple acquisitions using InSAR quality parameters. IEEE Journal of Selected Topics in Applied Earth Observations and Remote Sensing 9, 1047–1057.

Hawker, L., Bates, P., Neal, J., Rougier, J., 2018a. Perspectives on digital elevation model (DEM) simulation for flood modeling in the absence of a high-accuracy open access global DEM. Front. Earth Sci. 6.

Hawker, L.P., Rougier, J., Neal, J., Bates, P., Archer, L., Yamazaki, D., 2018b. Implications of simulating global digital elevation models for flood inundation studies. Water Resour. Res. 54 (10), 7910–7928.

Höhle, J., Höhle, M., 2009. Accuracy assessment of digital elevation models by means of robust statistical methods. ISPRS J. Photogramm. Remote Sens. 64, 398–406.

Holmes, K.W., Chadwick, O.A., Kydriakidis, P.C., 2000. Error in a USGS 30-meter digital elevation model and its impact on terrain modelling. J. Hydrol. 233, 154–173.

Horritt, M., Bates, P., 2002. Evaluation of 1D and 2D numerical models for predicting river flood inundation. J. Hydrol. 268, 87–99.

Hunter, G.J., Goodchild, M.F., 1997. Modelling the uncertainty of slope and aspect derived from spatial databases. Geophysical Analysis 29, 35–50.

InterMap, 2018. NextMap World 10. https://www.intermap.com/data/nextmap.

Jarvis, A., Reuter, H.I., Nelson, A., Guevara, E., 2008. Hole-filled SRTM for the Globe Version 4. http://srtm.csi.cgiar.org.

Jongman, B., Ward, P.J., Aerts, J.C.J.H., 2012. Global exposure to river and coastal flooding: long term trends and changes. Glob. Environ. Chang. 22, 823–835.

Kienzle, S., 2004. The effect of DEM raster resolution on first order, second order and

compound terrain derivatives. Trans. GIS 8, 83–111.
Krieger, G., Moreira, A., Fiedler, H., Hajnsek, I., Werner, M., Zink, M., 2007. TanDEM-X: a satellite formation for high-resolution SAR interferometry. IEEE Trans. Geosci. Remote Sens. 45, 3317–3340.
Kubanek, J., Westerhaus, M., Schenk, A., Aisyah, N., Brotopuspito, K.S., Heck, B., 2015. Volumetric change quantification of the 2010 Merapi eruption using TanDEM-X InSAR. Remote Sens. Environ. 164, 16–25.
Kydriakidis, P.C., Shortridge, A., Goodchild, M.F., 1999. Geostatistics for conflation and accuracy assessment of digital elevation models. Int. J. Geogr. Inf. Sci. 13, 677–707.
LaLonde, T., Shortridge, A., Messina, J., 2010. The influence of land cover on shuttle radar topography mission (SRTM) elevations in low-relief areas. Trans. GIS 14, 461–479.
Malz, P., Meier, W., Casassa, G., Jaña, R., Skvarca, P., Braun, M., 2018. Elevation and mass changes of the southern Patagonia icefield derived from TanDEM-X and SRTM data. Remote Sens. 10.
Martone, M., Rizzoli, P., Wecklich, C., González, C., Bueso-Bello, J.-L., Valdo, P., Schulze, D., Zink, M., Krieger, G., Moreira, A., 2018. The global forest/non-forest map from TanDEM-X interferometric SAR data. Remote Sens. Environ. 205, 352–373.
Mason, D.C., Trigg, M., Garcia-Pintado, J., Cloke, H.L., Neal, J.C., Bates, P.D., 2016. Improving the TanDEM-X Digital Elevation Model for flood modelling using flood extents from Synthetic Aperture Radar images. Remote Sens. Environ. 173, 15–28.
Maune, D. (Ed.), 2007. Digital Elevation Model Technologies and Applications: The Dem Users Manual. American Society for Photogrammetry and Remote Sensing.
Monckton, C., 1994. An Investigation into the Spatial Structure of Error in Digital Elevation Data. Taylor and Francis, London, UK.
Nardi, F., Annis, A., Di Baldassarre, G., Vivoni, E.R., Grimaldi, S., 2019. GFPLAIN250m, a global high-resolution dataset of Earth's floodplains. Sci Data 6, 180309.
NOAA, 2018. vdatum. National Oceanic and Atmospheric Administration.
O'Loughlin, F.E., Paiva, R.C.D., Durand, M., Alsdorf, D.E., Bates, P.D., 2016. A multi-sensor approach towards a global vegetation corrected SRTM DEM product. Remote Sens. Environ. 182, 49–59.
PlanetObserver, 2015. PlanetDEM 30 Plus. https://www.planetobserver.com/products/planetdem/planetdem-30/.
Poland, M.P., 2014. Time-averaged discharge rate of subaerial lava at Kīlauea Volcano, Hawai'i, measured from TanDEM-X interferometry: implications for magma supply and storage during 2011–2013. Journal of Geophysical Research: Solid Earth 119, 5464–5481.
Rankl, M., Braun, M., 2016. Glacier elevation and mass changes over the central Karakoram region estimated from TanDEM-X and SRTM/X-SAR digital elevation models. Ann. Glaciol. 57, 273–281.
Rexer, M., Hirt, C., 2014. Comparison of free high resolution digital elevation data sets (ASTER GDEM2, SRTM v2.1/v4.1) and validation against accurate heights from the Australian National Gravity Database. Aust. J. Earth Sci. 61, 213–226.
Rizzoli, P., Martone, M., Gonzalez, C., Wecklich, C., Borla Tridon, D., Bräutigam, B., Bachmann, M., Schulze, D., Fritz, T., Huber, M., Wessel, B., Krieger, G., Zink, M., Moreira, A., 2017. Generation and performance assessment of the global TanDEM-X digital elevation model. ISPRS J. Photogramm. Remote Sens. 132, 119–139.
Robinson, N., Regetz, J., Guralnick, R.P., 2014. EarthEnv-DEM90: a nearly-global, void-free, multi-scale smoothed, 90m digital elevation model from fused ASTER and SRTM data. ISPRS J. Photogramm. Remote Sens. 87, 57–67.
Rodriguez, E., Morris, C.S., Belz, J.E., 2006. A global assessment of the SRTM performance. Photogramm. Eng. Remote Sens. 72, 249–260.
Rossi, C., Gernhardt, S., 2013. Urban DEM generation, analysis and enhancements using TanDEM-X. ISPRS J. Photogramm. Remote Sens. 85, 120–131.
Rossi, C., Minet, C., Fritz, T., Eineder, M., Bamler, R., 2016. Temporal monitoring of subglacial volcanoes with TanDEM-X — application to the 2014–2015 eruption within the Bárðarbunga volcanic system, Iceland. Remote Sens. Environ. 181, 186–197.
Rott, H., Floricioiu, D., Wuite, J., Scheiblauer, S., Nagler, T., Kern, M., 2014. Mass changes of outlet glaciers along the Nordensjköld Coast, northern Antarctic Peninsula, based on TanDEM-X satellite measurements. Geophys. Res. Lett. 41, 8123–8129.
Sampson, C.C., Smith, A.M., Bates, P.D., Neal, J.C., Alfieri, L., Freer, J.E., 2015. A high-resolution global flood hazard model. Water Resour. Res. 51, 7358–7381.
Santoro, M., Kirches, G., Wevers, J., Boettcher, M., Brockmann, C., Lamarche, C., Bontemps, S., Moreau, I., 2017. Land Cover CCI Product User Guide Version 2.0.
Schlund, M., von Poncet, F., Hoekman, D.H., Kuntz, S., Schmullius, C., 2014. Importance of bistatic SAR features from TanDEM-X for forest mapping and monitoring. Remote Sens. Environ. 151, 16–26.
Shortridge, A., 2006. Shuttle radar topography mission elevation data error and its relationship to land cover. Cartogr. Geogr. Inf. Sci. 33, 65–75.
Shortridge, A., Messina, J., 2011. Spatial structure and landscape associations of SRTM error. Remote Sens. Environ. 115, 1576–1587.
Simard, M., Pinto, N., Fisher, J.B., Baccini, A., 2011. Mapping forest canopy height globally with spaceborne lidar. J. Geophys. Res. 116.
Tachikawa, T., Hato, M., Kaku, M., Iwasaki, A., 2011a. Characteristics of ASTER GDEM version 2. In: Geoscience and Remote Sensing Symposium (IGARSS). IEEE, pp. 3657–3660.
Tachikawa, T., Kaku, M., Iwasaki, A., Gesch, D.B., Oimoen, M., Zhang, Z., Danielson, J.J., Krieger, T., Curtis, B., Haase, J., Abrams, M., Crippen, R., Carabajal, C.C., 2011b. ASTER Global Digital Elevation Model Version 2 – Summary of Validation Results. NASA.
Tadono, T., Ishida, H., Oda, F., Naito, S., Minakawa, K., Iwamoto, H., 2014. Precise global DEM generation by ALOS PRISM. ISPRS Annals of Photogrammetry, Remote Sensing and Spatial Information Sciences II-4, 71–76.
Tadono, T., Nagai, H., Ishida, H., Oda, F., Naito, S., Minakawa, K., Iwamoto, H., 2016. Generation of the 30 M-mesh global digital surface model by Alos Prism. ISPRS - International Archives of the Photogrammetry, Remote Sensing and Spatial Information Sciences XLI-B4, 157–162.
Takaku, J., Tadono, T., 2017. Quality updates of 'AW3D' global DSM generated from ALOS PRISM. In: Geoscience and Remote Sensing Symposium (IGARSS). IEEE, Fort Worth, TX, USA.
Takaku, J., Tadono, T., Tsutsui, K., Ichikawa, M., 2016. Validation of "Aw3d" global Dsm generated from Alos Prism. ISPRS Annals of Photogrammetry, Remote Sensing and Spatial Information Sciences III-4, 25–31.
Tobler, W.R., 1970. A computer movie simulating urban growth in the Detroit Region. Econ. Geogr. 46, 234–240.
Vaze, J., Teng, J., Spencer, G., 2010. Impact of DEM accuracy and resolution on topographic indices. Environ. Model Softw. 25, 1086–1098.
Wechsler, S.P., 2007. Uncertainties associated with digital elevation models for hydrologic applications: a review. Hydrol. Earth Syst. Sci. 11, 1481–1500.
Wechsler, S.P., Knoll, C.N., 2006. Quantifying DEM uncertainty and its effect on topographic parameters. Photogramm. Eng. Remote Sens. 9, 1081–1090.
Wendleder, A., Wessel, B., Roth, A., Breunig, M., Martin, K., Wagenbrenner, S., 2013. TanDEM-X water indication mask: generation and first evaluation results. IEEE Journal of Selected Topics in Applied Earth Observations and Remote Sensing 6, 171–179.
Wessel, B., 2016. TanDEM-X Ground Segment DEM Products Specification Document. EOC – Earth Observation Center, Oberpfaffenhofen, Germany, pp. 46.
Wessel, B., Huber, M., Wohlfart, C., Marschalk, U., Kosmann, D., Roth, A., 2018. Accuracy assessment of the global TanDEM-X digital elevation model with GPS data. ISPRS J. Photogramm. Remote Sens. 139, 171–182.
Wing, O.E.J., Bates, P.D., Smith, A.M., Sampson, C.C., Johnson, K.A., Fargione, J., Morefield, P., 2018. Estimates of present and future flood risk in the conterminous United States. Environ. Res. Lett. 13.
Wood, J.D., 1996. The geomorphological characterisation of digital elevation models. In: Department of Geography. University of Leicester, Leicester, pp. 466.
Yamazaki, D., Ikeshima, D., Tawatari, R., Yamaguchi, T., O'Loughlin, F., Neal, J.C., Sampson, C.C., Kanae, S., Bates, P.D., 2017. A high-accuracy map of global terrain elevations. Geophys. Res. Lett. 44 (11), 5844–5853.
Zhao, X., Su, Y., Hu, T., Chen, L., Gao, S., Wang, R., Jin, S., Guo, Q., 2018. A global corrected SRTM DEM product for vegetated areas. Remote Sensing Letters 9, 393–402.
Zink, M., Bachmann, M., Brautigam, B., Fritz, T., Hajnsek, I., Moreira, A., Wessel, B., Krieger, G., 2014. TanDEM-X: the new global DEM takes shape. IEEE Geoscience and Remote Sensing Magazine 2, 8–23.
Zwally, H.J., Schutz, R., Bentley, C., Bufton, J., Herring, T., Minster, J., Spinhirne, J., Thomas, R., 2009. GLAS/ICESat L2 Global Land Surface Altimetry Data.